Bull. Chem. Soc. Ethiop. **2026**, 40(10), 2265-2286.
DOI: https://dx.doi.org/10.4314/bcse.v40i10.15

ISSN 1011-3924
Printed in Ethiopia
Online ISSN 1726-801X

PROFILING PHENOLIC CONSTITUENTS AND TISSUE-SPECIFIC BIOLOGICAL ACTIVITIES OF THE EDIBLE MUSHROOM *PLEUROTUS OSTREATUS*: EVIDENCE FROM IN *VITRO* AND IN SILICO STUDIES

Salma O. Jadallah[1*], Yassmin F. El Greeby[1], Mohammed Alakib[2*], Md. Sakib Al Hasan[3], Mustapha Belaidi[4,5], Saleh Bufarwa[6], Marei El-Ajaily[7], Leila M. Abbass[8]

[1]Department of Botany, faculty of sciences, University of Omar Al-Mukhtar, Al-bayda, Libya
[2]Department of Chemistry, faculty of sciences, Tobruk University, Tobruk, Libya
[3]Department of Pharmacy, Gopalganj Science and Technology University, Gopalganj 8100, Bangladesh
[4]Physical Chemistry Department, Chemistry Faculty, University of Sciences and Technologies of Oran (USTO), Laboratory of Process Engineering and Environment (LIPE), BP 1503 Oran 31000, Oran, Algeria
[5]Chemistry Laboratory Environment and Sustainable Department, Ahmed Zabana University, Relizane, Algeria
[6]Department of Chemistry, faculty of sciences, University of Omar Al-Mukhtar, Al-bayda, Libya
[7]Department of Chemistry, faculty of sciences, University of Benghazi, Libya
[8]Department of Chemistry, Faculty of Science, Zagazig University, 44519, Zagazig, Egypt

(Received January 27, 2026; Revised May 22, 2026; Accepted July 6, 2026)

ABSTRACT. *Pleurotus ostreatus* is an edible mushroom rich in bioactive phenolics. This study investigates the tissue-specific phenolic profiles and biological activities of cap and stipe extracts from a Libyan wild *P. ostreatus* using HPLC-DAD, experimental bioassays, and computational analysis. HPLC-DAD revealed a clear tissue-dependent distribution; the cap extract was dominated by chlorogenic (55.07%) and gallic acids (35.63%), while the stipe extract showed a more diversified composition. Consequently, the cap exhibited higher total phenolic/flavonoid contents and stronger antioxidant activity (DPPH IC_{50} = 16.74 µg/mL). Conversely, the stipe demonstrated pronounced anti-inflammatory activity, achieving 93.1% inhibition of protein denaturation (IC_{50} = 5.13 µg/mL), comparable to diclofenac. Both extracts showed antimicrobial activity and selective cytotoxicity against HepG2 cells, with minimal toxicity toward normal WI-38 fibroblasts. Molecular docking and density functional theory (DFT) analyses supported these findings, confirming stable interactions of major phenolics with the Bcl-2 protein. These results emphasize the importance of tissue-specific evaluation of mushroom extracts.

KEY WORDS: Antioxidant activity, Cap and stipe, Cytotoxicity, Molecular docking, *Pleurotus ostreatus*

INTRODUCTION

Natural products remain an important source of bioactive compounds with potential applications in functional foods, nutraceuticals, and pharmaceutical research [1, 2]. Among natural resources, edible mushrooms have attracted considerable scientific interest because they contain diverse secondary metabolites, polysaccharides, phenolic compounds, vitamins, minerals, and other biologically active constituents [3, 4]. These compounds are frequently associated with antioxidant, anti-inflammatory, antimicrobial [5, 6], immunomodulatory, and anticancer properties, making mushrooms valuable candidates for the discovery of natural health-promoting agents [7-9]. Among edible mushrooms, *Pleurotus ostreatus*, commonly known as oyster mushroom, is one of the most widely consumed and studied species due to its nutritional value,

*Corresponding author. E-mail: mohammed.alakib@tu.edu.ly

ease of cultivation, and reported medicinal properties [10, 11]. Previous studies have shown that *P. ostreatus* contains several classes of bioactive molecules, including phenolic acids, flavonoids, polysaccharides, and terpenoid-like compounds, which may contribute to its biological activities [12,13]. In particular, phenolic compounds are important because of their ability to donate electrons or hydrogen atoms, chelate metal ions, modulate oxidative stress, and interact with biological targets involved in inflammation and cell survival [14, 15]. Although several studies have investigated the biological potential of *P. ostreatus*, most available reports have focused on whole fruiting-body extracts or cultivated samples, while less attention has been given to tissue-specific differences between mushroom parts [16-18]. The cap and stipe may differ in their metabolic composition because they perform different biological functions during mushroom development. Therefore, evaluating these tissues separately may provide a more accurate understanding of how bioactive compounds are distributed within the mushroom and how this distribution influences biological activity [19, 20]

In Libya, wild *P. ostreatus* represents an underexplored biological resource [21]. The first Libyan specimen from the Marwa region has been documented in the GenBank database, providing evidence of its local biodiversity. However, limited information is available regarding its phenolic profile, tissue-specific biochemical composition, and associated biological activities. This lack of information represents an important research gap, especially because local environmental conditions may influence the accumulation of bioactive metabolites and, consequently, the biological properties of the mushroom [22, 23]. Complementing experimental assessments, computational approaches have become valuable tools for interpreting the biological behavior of natural and synthetic bioactive compounds [4, 24].

In particular, molecular docking and density functional theory (DFT) analyses can provide mechanistic insight into ligand–receptor interactions, electronic distribution, molecular stability, and possible reactive sites [25, 26]. Recent studies have demonstrated the usefulness of combining experimental characterization with computational analysis to evaluate the biological potential of newly designed compounds, including pyrazole- and tetrazole-based derivatives with antifungal activity [27]. Similarly, integrated green-synthesis and computational approaches have been increasingly applied in biomedical research, including the development of metallic nanoparticles for cancer-related applications [28, 29].

Therefore, combining HPLC-DAD profiling, in vitro biological assays, DFT calculations, and molecular docking can provide a more comprehensive understanding of the bioactive potential of *P. ostreatus* extracts and help relate their phenolic composition to observed antioxidant, anti-inflammatory, antimicrobial, and cytotoxic activities. Therefore, the novelty of the present study lies in the integrated tissue-specific profiling of Libyan wild P. ostreatus, combining HPLC-DAD analysis, antioxidant, anti-inflammatory, antimicrobial, and cytotoxic assays with Density functional theory (DFT) and molecular docking studies. This approach allows the biological potential of each mushroom part to be evaluated separately and provides a clearer understanding of how phytochemical distribution contributes to functional activity. Such in-silico analyses help prioritize compounds and targets for further laboratory validation. Therefore, this study aims to investigate the Libyan *P. ostreatus* strain PP029071 by assessing its bioactive compounds and biological activities, including anti-inflammatory, antioxidant, antimicrobial, and cytotoxic effects, complemented by molecular docking to explore potential protein targets. This integrated approach provides a systematic framework for evaluating the therapeutic potential of the local strain and its possible applications in medicine and industry.

EXPERIMENTAL

Chemical and reagent

Methanol (99.85%), ethanol (99.9%), distilled water, hydrochloric acid (HCl, 37%), chloroform ($CHCl_3$, 99.8%), phosphoric acid (H_3PO_4, 85%), sodium hydroxide (NaOH, 98%), sodium chloride (NaCl, 99%), Coomassie Brilliant Blue G-250 ($C_{47}H_{48}N_3NaO_7S_2$, ≥ 95%), petroleum ether, Bradford reagent solution, gallic acid (99%), quercetin (98%), glucose (99%), Folin–Ciocalteu reagent, sodium carbonate (Na_2CO_3, ≥ 99%), phenol (≥ 99%), sulphuric acid (H_2SO_4, 95-98%), sodium nitrite ($NaNO_2$, ≥ 99%), aluminum chloride ($AlCl_3$, ≥ 98%), bromocresol green ($C_{21}H_{14}Br_4O_5S$, 95%), sodium phosphate dibasic (Na_2HPO_4, 99%), citric acid (99.5%), atropine standard (≥ 98%), and vanillin (99%), all purchased from Sigma-Aldrich (USA).

Instruments and apparatus

An Agilent Technologies Agilent 1260 Infinity high-performance liquid chromatography system equipped with a diode array detector (Santa Clara, CA, USA) was used for HPLC-DAD analysis. Total phenolic and flavonoid contents were determined using a Jenway JENWAY 6305 UV/Vis spectrophotometer (Staffordshire, UK). Extract concentration was carried out using a rotary evaporator (Heidolph, Schwabach, Germany). Ultrasonic extraction was performed using an ultrasonic bath (Elma, Singen, Germany). Cytotoxicity assays were conducted using a microplate reader (BioTek, Winooski, VT, USA) and a CO_2 incubator (Thermo Scientific, Waltham, MA, USA). Additional routine laboratory equipment included an analytical balance, pH meter, centrifuge, and micropipettes.

Mushroom material

Wild samples of the oyster mushroom *P. ostreatus* was collected from the Marawa region, Al-Jabal Al-Akhdar province, northeastern Libya, between December 2024 and March 2025. The botanical identity was confirmed based on morphological and ecological characteristics. Samples were cleaned with distilled water, and the cap and stipe were separated. The materials were dried at 60 °C for 24 h, ground into a fine powder, and stored in airtight dark containers until use.

Preparation of mushroom extracts

The dried powder of *P. ostreatus* (cap and stipe separately) was subjected to extraction using ethanolic extracts were prepared by macerating 20 g of powdered sample with 200 mL of 85% (v/v) ethanol in sealed containers at room temperature for 24 h. The mixtures were then subjected to sonication at 40 °C for 60 min to enhance extraction efficiency. After extraction, the solutions were filtered, and the filtrates were concentrated under reduced pressure using a rotary evaporator at 40 °C to obtain crude extracts. Different extract concentrations (12.5, 25, 50, 75%, and 100%) were prepared for subsequent analyses [30].

Determination total phenolic and flavonoid content

The total phenolic and flavonoid contents were quantified using a JENWAY 6305 UV/Vis spectrophotometer according to previously described procedures. The complete analytical protocols, including reagent preparation, calibration curve generation, assay conditions, and calculation approaches, are provided in the Supplementary Material. Phenolic content of the extracts was calculated using the gallic acid calibration curve and expressed as gallic acid equivalents (mg GAE/g dry extract), whereas flavonoid content was determined using the

quercetin calibration curve and expressed as quercetin equivalents (mg QE/g dry extract). All experiments were performed in triplicate, and data are presented as mean ± standard deviation.
High-performance liquid chromatography analysis

HPLC analysis was performed using an Agilent 1260 series system. Separation was achieved on a Zorbax Eclipse Plus C8 column (4.6 × 250 mm, 5 μm). The mobile phase consisted of solvent A (water) and solvent B (acetonitrile containing 0.05% trifluoroacetic acid), delivered at a flow rate of 0.9 mL/min. The elution was carried out using a linear gradient program as follows: 0 min (82% A), 0–1 min (82% A), 1-11 min (75% A), 11–18 min (60% A), 18–22 min (82% A), and 22-24 min (82% A). Detection was performed at 280 nm using a multi-wavelength detector. The injection volume was 5 μL for each sample, and the column temperature was maintained at 40 °C.

Biological activity

Anti-inflammatory activity

The anti-inflammatory activity was evaluated using the BSA denaturation assay. A volume of 50 μL of the sample, prepared at various concentrations (1.56, 3.12, 6.25, 12.5, 25, 50, 100, and 200 μg/mL), was added to 450 μL of a 1% aqueous solution of bovine serum albumin (BSA). The pH of the reaction mixture was adjusted to 6.3 using 1N HCl [10].

Antimicrobial activity

The antimicrobial activity of *P. ostreatus* cap and stipe extracts was evaluated using complementary methods, including agar well diffusion, disc diffusion, and Minimum inhibitory concentration (MIC)/ Minimum bactericidal concentration (MBC)/ Minimum fungicidal concentration (MFC) determination. These assays were used to provide both preliminary screening and concentration-dependent evaluation of antimicrobial effects. The agar well diffusion assay was used as an initial qualitative screening method to detect the presence of antimicrobial activity through inhibition-zone formation. The disc diffusion assay was used to compare the inhibitory effects of different extract concentrations under standardized diffusion conditions. MIC and MBC/MFC determinations were performed to estimate the lowest concentration required to inhibit visible microbial growth and to assess the bactericidal or fungicidal potential of the extracts.

Agar well diffusion assay

The agar well diffusion method was used for preliminary antimicrobial screening. Bacterial strains were cultured on Mueller–Hinton agar, whereas fungal and yeast strains were cultured on Sabouraud dextrose agar. Microbial suspensions were adjusted to the 0.5 McFarland standard and uniformly swabbed onto the agar surface. Wells of 6 mm diameter were aseptically punched into the agar plates, and 100 μL of each extract solution was added to each well. Gentamicin was used as the positive control for bacterial strains, fluconazole was used as the positive control for fungal strains, and the extraction solvent served as the negative control. Plates were incubated at 37 °C for 24 h for bacteria and at 28-30 °C for 48 h for fungi. Antimicrobial activity was evaluated by measuring the diameter of the inhibition zone around each well in millimeters [32].

Disc diffusion assay

The disc diffusion assay was used to evaluate the concentration-dependent antimicrobial response of the extracts. Sterile filter-paper discs of 6 mm diameter were impregnated with 20 μL of cap or stipe extract at different concentrations. The discs were then placed onto agar plates previously

inoculated with standardized microbial suspensions. Discs containing gentamicin or fluconazole were used as positive controls, while discs containing only the solvent were used as negative controls. Plates were incubated at 37 °C for 18-24 h for bacterial strains and at 28-30 °C for 48 h for fungal strains. After incubation, the inhibition zones around the discs were measured in millimeters. The results were expressed as mean inhibition zone diameter ± standard deviation from three independent replicates [33, 34].

Determination of MIC, MBC, and MFC

The minimum inhibitory concentration (MIC) was determined as the lowest extract concentration that prevented visible microbial growth. The minimum bactericidal concentration (MBC) or minimum fungicidal concentration (MFC) was determined as the lowest concentration that resulted in no visible microbial growth after subculturing onto fresh agar medium. These values were used to provide a quantitative estimate of antimicrobial potency and to distinguish inhibitory effects from bactericidal or fungicidal effects. Because the tested samples were crude extracts, the MIC and MBC/MFC values were interpreted cautiously and compared with standard antimicrobial agents only as reference controls, not as evidence of equivalent potenc [35].

Antioxidant activity by DPPH radical scavenging method

Free radical scavenging activity of different extracts of leaves plant were measured by 1, 1-diphenyl-2-picryl hydrazyl (DPPH) [36]. In brief, 0.1 mM solution of DPPH in ethanol was prepared. This solution (1 mL) was added to 3 mL. of different extracts in ethanol at different concentrations (3.9, 7.8, 15.62, 31.25, 62.5, 125, 250, 500, 1000 µg/mL). Here, only those extracts are used which are Solubilize in ethanol and their various concentrations were prepared by dilution method. The mixture was shaken vigorously and allowed to stand at room temperature for 30 min. then; absorbance was measured at 517 nm. by using spectrophotometer (UV-VIS milton roy). Reference standard compound being used was ascorbic acid and experiment was done in triplicate.16 The IC_{50} value of the sample, which is the concentration of sample required to inhibit 50% of the DPPH free radical, was calculated using Log dose inhibition curve. Lower absorbance of the reaction mixture indicated higher free radical activity. The percent DPPH scavenging effect was calculated by using following equation: DPPH scavenging effect (%) = A0 - A 1 / A0 × 100. Where A0 was the absorbance of control reaction and A1 was the absorbance in presence of test or standard sample.

MTT assay

The cytotoxic and antiproliferative effects of the tested samples were evaluated using the MTT (3-(4,5-dimethylthiazol-2-yl)-2,5-diphenyltetrazolium bromide) assay following previously described procedures. Human hepatocellular carcinoma cells (HepG2) and normal human lung fibroblasts (WI-38) were seeded in 96-well plates at a density of 1×10^5 cells/mL (100 µL/well) and incubated at 37 °C for 24 h to allow monolayer formation. After removing the culture medium and washing the cells twice, two-fold serial dilutions of the samples were prepared in RPMI supplemented with 2% FBS, and 100 µL of each concentration were added to the wells; untreated wells served as controls. Following incubation at 37 °C, the wells were inspected microscopically for cytotoxic morphological alterations. MTT solution (5 mg/mL in PBS) was added (20 µL/well), and plates were shaken for 5 min and further incubated for 4 h to enable formazan crystal formation. The medium was discarded, crystals were dissolved in 200 µL DMSO, and absorbance was measured at 560 nm with background correction at 620 nm. Cell viability (%) was calculated relative to untreated controls, and IC_{50} values were derived from the dose–response curves.

Morphological assay

Cellular morphological alterations were assessed microscopically to support quantitative viability findings. Cytotoxic damage was indicated by loss of monolayer integrity, cell shrinkage, rounding, granulation, and detachment. Necrotic manifestations included nuclear swelling and chromatin flocculation, while apoptotic features were characterized by cellular shrinkage, nuclear condensation, and fragmentation.

Computational studies

Density functional theory analysis

The investigated compounds were initially built using GaussView 6.0, and their geometries, including bond lengths and three-dimensional structural parameters, were fully optimized using the Gaussian 09W software package [37]. The Becke three-parameter exchange functional combined with the Lee–Yang–Parr correlation functional (B3LYP) together with the 6-311G(d,p) basis set was employed to optimize the structures of the studied systems, providing an appropriate balance between computational cost and accuracy [38]. The optimized molecular geometries were verified to confirm the absence of imaginary frequencies, ensuring that the obtained structures correspond to true energy minima [39]. Frontier molecular orbital (FMO) analysis was subsequently performed to compute the energies of the highest occupied molecular orbital (HOMO) and the lowest unoccupied molecular orbital (LUMO), which are essential for understanding the electronic distribution, charge transfer characteristics, and chemical reactivity of the molecules [40]. In addition, several global quantum descriptors derived from conceptual density functional theory (DFT), including electronegativity (χ), chemical hardness (η), softness (σ), chemical potential (μ), electrophilicity index (ω), and maximum charge transfer (ΔN_{max}), were calculated in order to evaluate the stability, reactivity, and potential biological behavior of the compounds [41]. The energy gap (ΔE = ELUMO − EHOMO) together with HOMO–LUMO distributions was further used to provide insight into the most probable reactive sites toward electrophilic and nucleophilic attacks, thereby supporting the prediction of their possible biochemical interactions [42].

Molecular docking

Ligand preparation

The three-dimensional structures of Bcl-2-IN-13 (Co-crystal) (PubChem CID: 71527841), CFA (PubChem CID: 689043), CTC (PubChem CID: 9064), CRG (PubChem CID: 1794427), ELG (PubChem CID: 5281855), GA (PubChem CID: 370), RMC (PubChem CID: 5281792) and VNL (PubChem CID: 1183) were downloaded in SDF format from the PubChem online chemical database. The Chem3D 22.0.0 software tool was then used to reduce these chemical agents utilizing Allinger's force field (MM2) approach [43].

Protein selection and preparation

Based on previous study, the Bcl-2 protein was selected for molecular docking and receptor–ligand interaction analysis. The RCSB Protein Data Bank provided the Bcl-2 protein (PDB ID: 4IEH). To reduce any possible docking interference, the receptors were then optimized. This was accomplished by utilizing the PyMol software tool (version 2.4.1) to remove undesired protein chains and superfluous elements from the protein sequence, such as lipids, water molecules, and heteroatoms [44]. In the end, the SwissPDB Viewer software was utilized to save the PDB file for molecular docking, decrease energy, and optimize the shape of the receptors using the GROMOS96 force field [19].

Molecular docking and visualization protocol

The selected ligands were molecularly docked with the Bcl-2 protein receptors. To anticipate the active binding potential of the drugs against the active sites of receptors, molecular docking was carried out using the PyRx software tool [20]. The receptor and the ligand are enclosed in a grid box for docking; the grid box dimensions were set at 38.15 × 35.59 × 25.00 values along the x-, y-, and z-axes, and the computation was performed in 200 steps. The optimal ligand-protein pose was gathered in PDB format for binding interaction analysis, and the docking potential result was saved in CSV format. The Discovery Studio Visualizer (v21.1.020298) was used to observe the interactions between the ligand-receptor and the receptor's active site [37]. Subsequently, the amino acid (AA) residues, bond types, hydrogen bonds (HB), hydrophobic bonds (HP), length of HB, and other bond types for each ligand-receptor interaction were documented.

Docking validation

Docking validation assesses the precision of molecular docking outcomes to guarantee the biological significance of ligand-target protein interactions [25]. In this study, we redocked with the co-crystal against the protein active site for the molecular docking validation. The active location where co-crystals bind to proteins has been our focus.

Statistical analysis

All experimental data were analyzed using IBM SPSS Statistics (version 26). Quantitative results are presented as mean ± standard deviation. Differences in chemical and biochemical parameters among multiple groups were assessed using one-way ANOVA followed by Tukey's HSD post-hoc test, while the effects of two independent factors (species and mushroom part) and their interaction were evaluated via two-way ANOVA. Pearson correlation coefficients were calculated to examine linear relationships between variables, such as total phenolic content and antioxidant activity or extract concentration and inhibition zone diameter. The reliability and precision of repeated measurements were assessed using standard deviation and standard error, and standard curves for phenols, flavonoids, and carbohydrates were validated through linear regression, with R^2 values confirming analytical accuracy. Statistical significance was considered at $p < 0.05$ throughout the study [4,10].

RESULTS AND DISCUSSION

Profiling of phenolic constituents

The phenolic composition of *P. ostreatus* cap and stipe extracts was investigated using HPLC with a diode array detector at 280 nm as shown in Figure 1 [14]. The relative abundance of each phenolic compound was expressed as the normalized percentage of the total chromatographic peak area. This approach allowed a comparative evaluation of the tissue-specific distribution of bioactive phenolics. As summarized in Table 1, the cap extract exhibited a clearly dominant presence of chlorogenic acid (55.07% of total peak area), followed by gallic acid (35.63%) and cinnamic acid (4.34%), whereas the remaining phenolics, including methyl gallate, syringic acid, rutin, ellagic acid, coumaric acid, rosmarinic acid, quercetin, and kaempferol, were present in minor proportions. In contrast, the stipe extract displayed a more heterogeneous phenolic profile, with ellagic acid (8.89%), vanillin (8.54%), rosmarinic acid (8.13%), cinnamic acid (6.67%), and hesperetin (6.11%) as the major contributors, alongside measurable levels of gallic acid, chlorogenic acid, catechin, caffeic acid, methyl gallate, syringic acid, rutin, coumaric acid, ferulic acid, naringenin, daidzein, quercetin, and kaempferol. Compounds showing 0.00% in the cap

chromatogram indicate undetectable levels under the applied HPLC conditions rather than absolute absence. Overall, these results reveal a tissue-dependent allocation of phenolic compounds, with the cap enriched in hydroxycinnamic and hydroxybenzoic acids and the stipe exhibiting a broader spectrum of bioactive phenolics (Figure S1). This distribution provides a strong basis for linking the cap extract to antioxidant and cytotoxic activities and the stipe extract to anti-inflammatory and antimicrobial effects, as observed in subsequent in vitro assays. The findings align with previous Pleurotus studies, which emphasize the role of chlorogenic, gallic, and ellagic acids in contributing to biological activities, while underscoring the impact of tissue-specific metabolite allocation on bioactive potential [4,11].

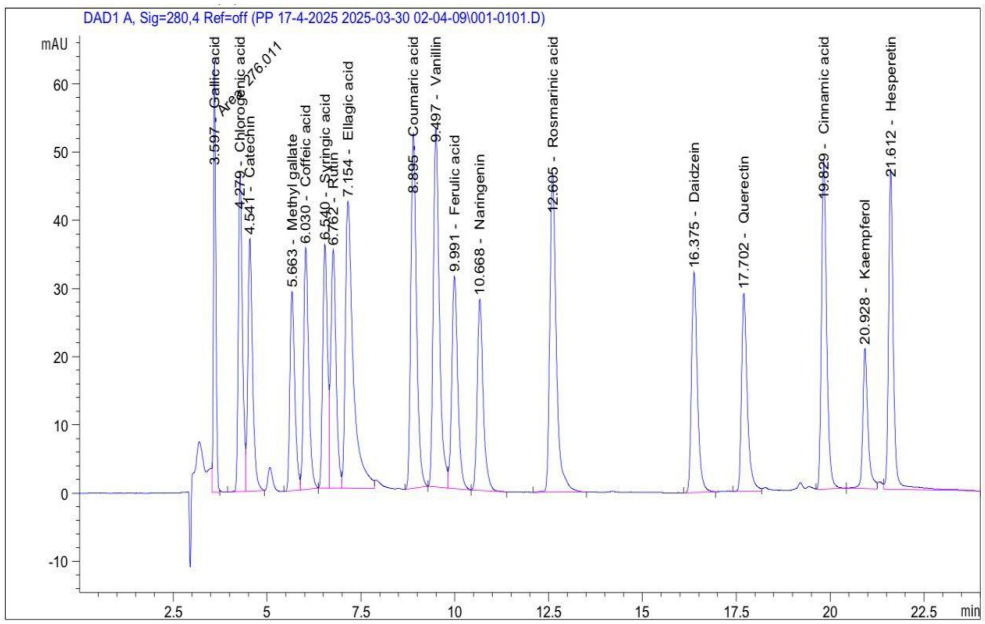

Figure 1. HPLC-DAD chromatograms *P. ostreatus* extracts.

Table 1. Unified HPLC-determined concentrations of phenolic compounds in *P. ostreatus* (cap and stipe).

Compound	Cap Retime (min)	Cap Area	Cap Area %	Cap Conc (µg/g)	Stipe Retime (min)	Stipe Area	Stipe Area %	Stipe Conc (µg/g)
Gallic acid	3.474	88.899	35.63	356.0	3.597	276.011	3.99	39.8
Chlorogenic acid	4.228	137.40	55.07	550.0	4.279	356.818	5.15	51.5
Catechin	4.402	0.000	0.00	0.0	4.541	323.033	4.67	46.7
Methyl gallate	5.658	1.320	0.53	5.3	5.663	264.594	3.82	38.2
Caffeic acid	5.858	0.000	0.00	0.0	6.030	334.094	4.83	48.3
Syringic acid	6.226	1.040	0.42	4.2	6.540	312.409	4.51	45.1
Rutin	6.691	1.079	0.43	4.3	6.762	343.907	4.97	49.7
Ellagic acid	6.900	1.689	0.68	6.8	7.154	615.657	8.89	88.9
Coumaric acid	8.506	3.295	1.32	13.2	8.895	547.680	7.91	79.1
Vanillin	9.291	0.000	0.00	0.0	9.497	590.890	8.54	85.4
Ferulic acid	9.788	0.000	0.00	0.0	9.991	345.814	5.00	50.0
Naringenin	10.521	0.000	0.00	0.0	10.668	310.304	4.48	44.8
Rosmarinic acid	12.181	1.466	0.59	5.9	12.605	562.734	8.13	81.3

Daidzein	16.175	0.000	0.00	0.0	16.375	349.792	5.05	50.5
Quercetin	18.178	1.158	0.46	4.6	17.702	308.877	4.46	44.6
Cinnamic acid	19.712	10.823	4.34	43.4	19.829	462.022	6.67	66.7
Kaempferol	20.871	1.333	0.53	5.3	20.928	195.065	2.82	28.2
Hesperetin	21.485	0.000	0.00	0.0	21.612	422.949	6.11	61.1

Total phenolic and flavonoid content

P. ostreatus was analyzed to assess the antioxidant activity of its cap and stipe parts (phenolic and flavonoid) [9]. The total phenolic content (TPC) was found in different parts of the mushroom; it is expressed in mg of gallic acid equivalent per gram (mg GAE/g). The cap had the highest value of TPC (26.99 mg GAE/g) followed by the stipe (17.77 mg GAE/g) (Table S1). This confirms the presence of more phenolics in the cap, as it is actively involved in the production of these spores and is more exposed to oxidative stress, which may trigger the production of antioxidant phenolics of low molecular weight. Gallic acid standards were prepared and then calibrated to prove the reliability of the UV–Vis spectrophotometric method. The absorbance was found to increase in a linear fashion with the concentration of gallic acid between 15.62–500 µg/mL. The corrected calibration curve was determined by plotting the concentration of gallic acid on the X-axis and absorbance on the Y-axis, on which the regression equation was $y = 0.00245x + 0.03586$, with $R^2 = 0.996$. This means that the linearity and precision for the determination of TPC are excellent (Figure 2).

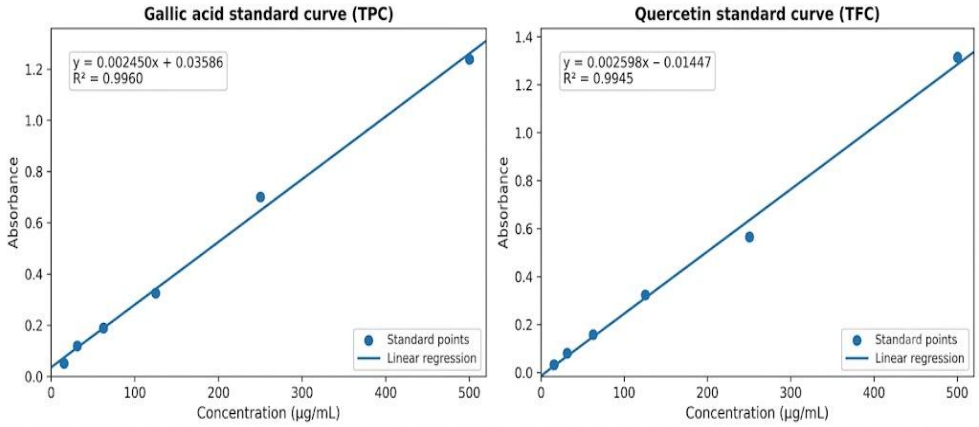

Figure 2. UV–Vis calibration curves of gallic acid and quercetin standards for TPC and TFC determination.

Biological activity

Anti-inflammatory activity

The anti-inflammatory performance of *P. ostreatus* extracts was evaluated in comparison with the standard reference drug diclofenac sodium [13], as shown in Figure 3 and detailed in Tables S2 and S3. Diclofenac exhibited the highest efficacy, achieving up to 98% inhibition and the lowest IC_{50} value (1.81 µg/mL), thereby confirming the validity and sensitivity of the protein denaturation model. When benchmarked against this standard, the stipe extract of *P. ostreatus* demonstrated remarkable potency, reaching 93.1% inhibition at 200 µg/mL and exhibiting a notably low IC_{50} value of 5.13 µg/mL, indicating strong drug-comparable biological activity. In

contrast, the cap extract showed relatively lower efficacy, with a maximum inhibition of 88.3% and a higher IC_{50} value of 12.33 µg/mL. This comparison clearly demonstrates two key observations: (i) the stipe of *P. ostreatus* is substantially more active than the cap, reflecting a higher concentration and/or stronger functionality of anti-inflammatory constituents in this tissue; and (ii) although diclofenac remains superior, the potency of the *P. ostreatus* stipe extract falls within a promising bioactive range, supporting its potential as a natural anti-inflammatory candidate. These findings emphasize the pharmacological relevance of *P. ostreatus*, particularly its stipe fraction, and justify further investigation to characterize its active compounds and validate its efficacy in vivo [5, 46].

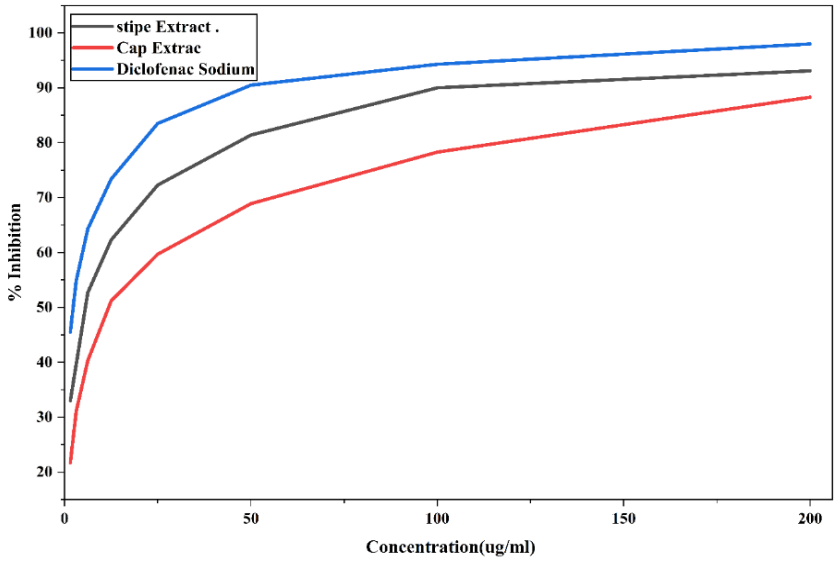

Figure 3. Anti-inflammatory activity and IC_{50} determination of *P. ostreatus* stipe extract.

Antioxidant activity

The antioxidant potential of methanolic extracts from *P. ostreatus*, including the cap and stipe, was evaluated using the DPPH radical scavenging method, with ascorbic acid as the reference standard [5]. As shown in Figure 4 and detailed in Table S4, both extracts exhibited strong, concentration-dependent radical scavenging activity. At the highest tested concentration (1000 µg/mL), the cap extract achieved 92.8% inhibition, slightly surpassing the stipe extract at 91.3%, while ascorbic acid reached 98.5% under similar conditions. The calculated IC_{50} values further reflected this trend, with the cap extract showing a lower IC_{50} (16.74 µg/mL) than the stipe (19.97 µg/mL), indicating higher radical scavenging efficiency in the cap fraction, although both extracts were less potent than ascorbic acid (IC_{50} = 2.88 µg/mL). The observed differences between cap and stipe extracts likely reflect variations in the concentration and composition of bioactive compounds, particularly phenolics and flavonoids, which are known contributors to antioxidant activity. The cap consistently demonstrated slightly superior activity across the concentration range, suggesting it as a richer source of these compounds. The high radical scavenging percentages at elevated concentrations, along with relatively low IC_{50} values, underscore the potential of both extracts as natural antioxidants. These findings align with previous reports on *P. ostreatus*, emphasizing the cap fraction as a more potent source of antioxidant compounds

suitable for nutraceutical, food preservation, or complementary therapeutic applications targeting oxidative stress [34, 47].

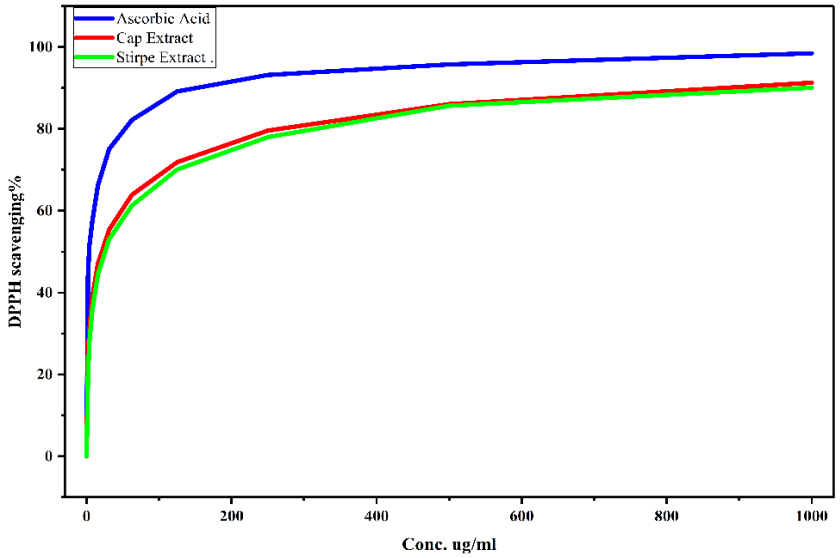

Figure 4. Concentration-dependent DPPH radical scavenging activity of *P. ostreatus* extracts in comparison with ascorbic acid.

Antimicrobial activity

As illustrated in Figure 5, the methanolic extracts of *P. ostreatus* demonstrated notable antimicrobial activity, with the stipe extract consistently outperforming the cap extract against all responsive pathogens. The stipe produced larger inhibition zones against *B. subtilis* (30 mm), *S. aureus* (23 mm), *K. pneumoniae* (25 mm), and *S. typhi* (26 mm), in several cases exceeding the activity of the standard antibiotic gentamicin (Table S5). Similarly, the stipe extract exhibited strong antifungal efficacy against *C. albicans* (27 mm), surpassing fluconazole, whereas both extracts were inactive against *A. niger*. These findings indicate that the antimicrobial potential of *P. ostreatus* is highly part dependent, with the methanolic extracts of *P. ostreatus* showing measurable antimicrobial activity against several tested microorganisms, with the stipe extract generally producing larger inhibition zones than the cap extract. However, the MIC and MBC/MFC values were relatively high compared with the standard antimicrobial agents, indicating that the crude extracts have weak to moderate antimicrobial potency rather than activity comparable to conventional antibiotics or antifungal drugs [48, 49].

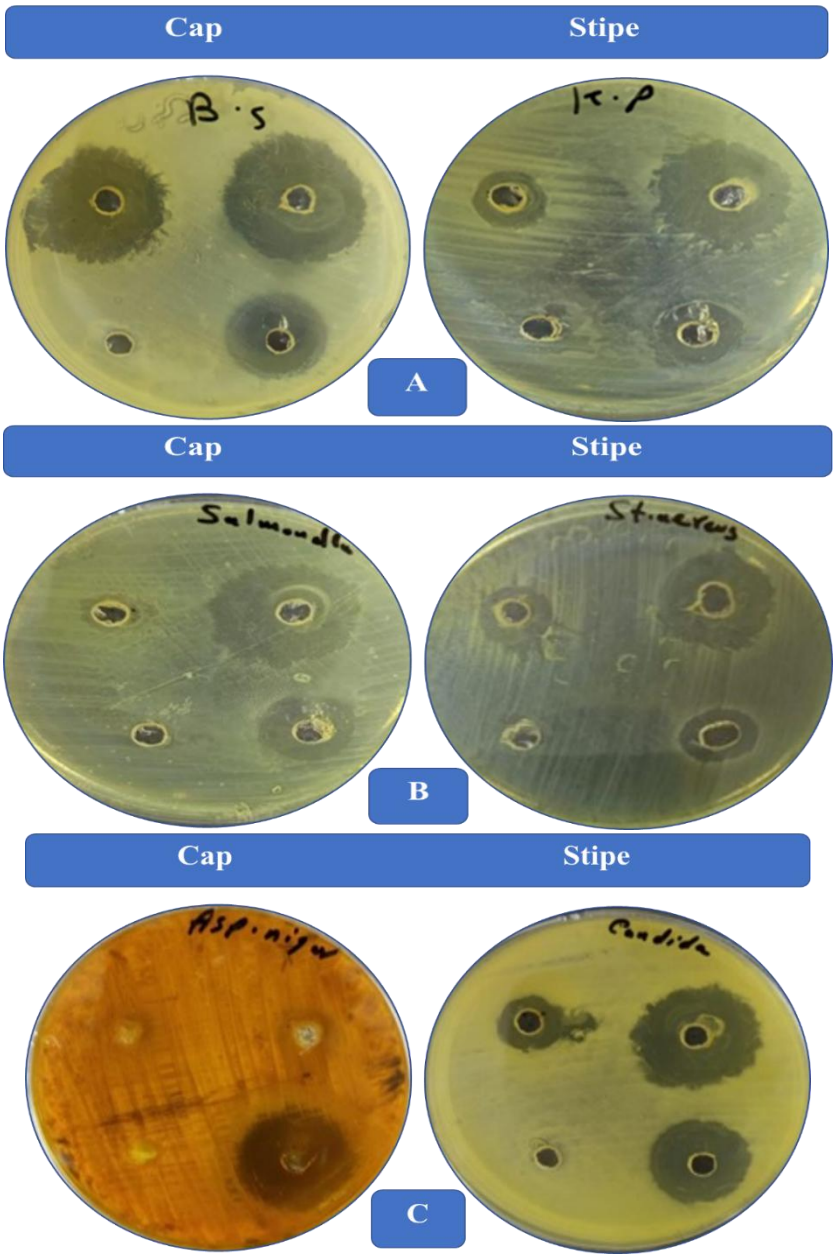

Figure 5. Antimicrobial and antifungal activity of methanolic extracts from *P. ostreatus* (cap and stipe) compared to standard antibiotics. (A) *B. subtilis* and *K. pneumoniae*; (B) *Salmonella spp.* and *S. aureus*; (C) *A. niger* and *C. albicans*.

The antimicrobial activity of *P. ostreatus* cap and stipe extracts was evaluated against selected bacterial and fungal strains. Although measurable inhibition zones were observed, the MIC and MBC/MFC values of the crude extracts were relatively high compared with the standard

antimicrobial agents, indicating moderate to weak antimicrobial potency (Figure S2). Therefore, the activity of these extracts should not be directly considered comparable to conventional antibiotics or antifungal drugs. The observed inhibitory effects may be attributed to the presence of phenolic and other secondary metabolites in the crude extracts; however, their relatively high effective concentrations suggest that the active constituents are either present at low abundance or may require purification to enhance antimicrobial efficacy. The stipe extract generally showed stronger activity than the cap extract against several tested microorganisms, suggesting tissue-dependent differences in antimicrobial constituents. Nevertheless, the lack of activity or limited activity against some microorganisms, particularly *A. niger*, indicates a restricted antimicrobial spectrum. Overall, these findings support the presence of antimicrobial bioactivity in *P. ostreatus* extracts but should be interpreted as preliminary evidence. Further studies involving bioassay-guided fractionation, compound isolation, and mechanism-of-action analysis are necessary to identify the active principles and evaluate their true antimicrobial relevance.

Cytotoxic activity

The cytotoxic effects of *P. ostreatus* cap and stipe extracts were evaluated against HepG2 hepatocellular carcinoma cells and WI-38 normal fibroblasts using the MTT assay. AS shown in Figure S3 and detailed in Table S6, both extracts induced concentration-dependent inhibition of HepG2 viability, with the cap extract showing higher potency (IC_{50} = 71.54 ± 0.39 µg/mL) compared to the stipe (IC_{50} = 112.70 ± 1.55 µg/mL), indicating enhanced cytotoxic activity in the cap likely due to a higher content of bioactive phenolics and terpenoids. In WI-38 fibroblasts, cytotoxicity was markedly lower, with IC_{50} values of 147.66 ± 0.22 µg/mL (cap) and 186.79 ± 2.47 µg/mL (stipe), yielding Selectivity Index (SI) values of 2.06 and 1.66, respectively, confirming preferential activity against malignant cells. For reference, the chemotherapeutic standard doxorubicin under identical conditions exhibited an IC_{50} of ~ 0.5 µg/mL in HepG2 cells and > 50 µg/mL in WI-38 cells, reflecting its higher potency but comparable selectivity. These findings highlight that *P. ostreatus* extracts, particularly from the cap, possess moderate yet selective anticancer activity, supporting their potential as safe, functional bioactive agents [30].

Morphological analysis

Morphological assessment provided supportive qualitative evidence for the viability data, as shown in Figure 6. HepG2 cells exposed to higher extract concentrations displayed hallmark features of cytotoxic damage, including monolayer disruption, cellular shrinkage, rounding, cytoplasmic granulation, and nuclear alterations. These structural changes are consistent with apoptotic and necrotic responses previously documented for mushroom-derived anticancer agents. In contrast, WI-38 cells retained comparatively preserved morphology at equivalent concentrations, further corroborating the reduced susceptibility of normal cells**.** The present findings demonstrate that *P. ostreatus* cap extract exhibits superior cytotoxic potency and selectivity compared with the stipe extract, highlighting the cap as a more promising bioactive fraction. The observed anticancer activity is likely associated with combined metabolic suppression and induction of regulated cell death mechanisms, potentially mediated by oxidative stress modulation, mitochondrial impairment, and signaling pathway disruption. While these results provide compelling preliminary evidence supporting the therapeutic relevance of *P. ostreatus* extracts, further mechanistic investigations such as apoptosis marker profiling, assessment of caspase activation, mitochondrial membrane potential analysis, and evaluation of oxidative stress indices are warranted. Additionally, broader cancer cell screening and in-vivo validation are essential to confirm pharmacological efficacy, biosafety, and translational applicability.

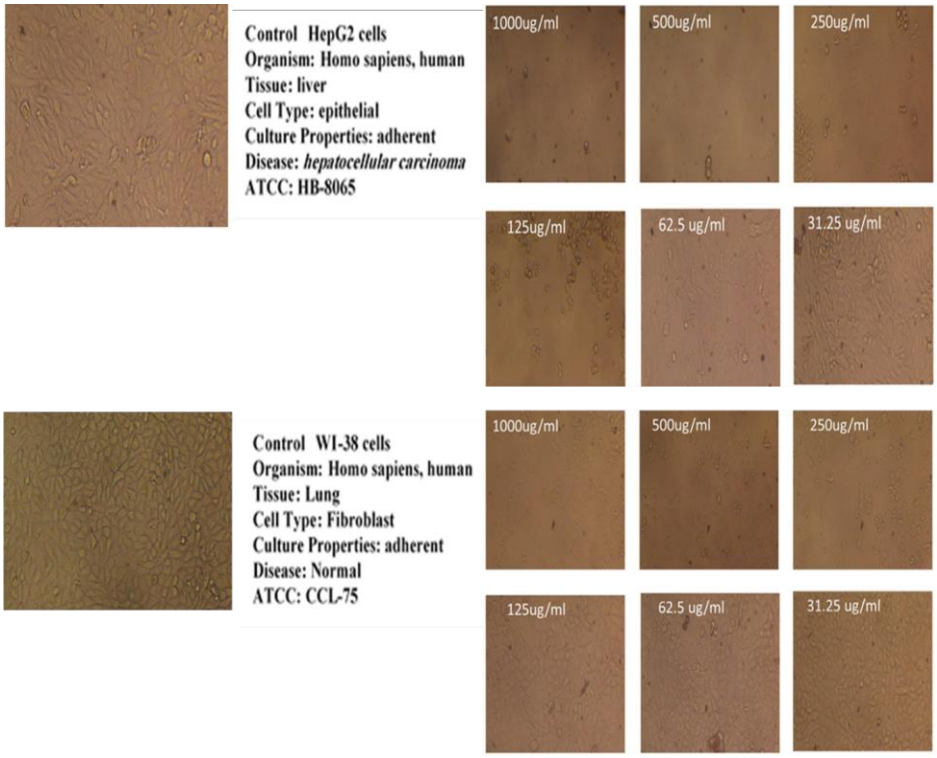

Figure 6. Morphological evaluation of HepG2 and WI-38 cells treated with *P. ostreatus* extracts.

Computational studies

Density functional theory analysis

The electronic structures of the major phenolic constituents of *P. ostreatus*, including caffeic acid, catechin, chlorogenic acid, rosmarinic acid, ellagic acid, vanillin, and gallic acid, were thoroughly investigated using DFT calculations at the B3LYP/6-311G(d,p) level. HOMO and LUMO energies, along with derived global reactivity descriptors, provide detailed insight into the electronic distribution, molecular reactivity, and potential interaction capabilities of these compounds are summarized in Table S7. The HOMO energies varied from -8.802 eV (vanillin) to -6.041 eV (ellagic acid), while LUMO energies ranged from -6.095 eV (chlorogenic acid) to -1.963 eV (ellagic acid). Consequently, the HOMO–LUMO energy gaps (ΔE) spanned 2.667-4.082 eV, highlighting the relative softness and electronic flexibility of hydroxycinnamic acids (caffeic, chlorogenic, rosmarinic), compared to the more rigid structures of catechin and ellagic acid. These differences suggest variation in the capacity for electron donation or acceptance, which is fundamental to potential molecular interactions**.** Global descriptors were calculated to quantify electronic characteristics and reactivity patterns. Electronegativity (χ) ranged from 4.002 to 7.429 eV, indicating substantial electron-attracting capacity across the phenolic compounds. Chemical hardness (η) values (1.333–2.041 eV) and corresponding softness (σ) (0.490–0.750 eV^{-1}) reveal that the hydroxycinnamic acids possess moderate hardness and enhanced polarizability, whereas catechin and ellagic acid are electronically more stable. Electrophilicity indices (ω) varied between 3.923 and 20.68 eV, while maximum charge transfer (ΔN_{max}) ranged

from 1.963 to 5.565, indicating significant potential for electron redistribution during molecular interactions. Analysis of frontier orbital distributions showed that the HOMO orbitals are predominantly localized on hydroxylated aromatic rings, suggesting that these regions are the primary sources for electron donation, whereas LUMO orbitals are concentrated on carbonyl and conjugated systems, defining the electron-accepting sites, as shown in Figure 7. This electronic topology provides a molecular rationale for differential reactivity and interaction tendencies among the phenolics**.** The DFT-derived electronic parameters indicate that these phenolic compounds possess diverse reactivity profiles, combining varying degrees of softness, electrophilicity, and electron transfer potential [20]. These properties establish a mechanistic basis for their subsequent bioactivity, allowing a direct and rational link to the observed anti-inflammatory, antioxidant, antimicrobial, and cytotoxic effects of *P. ostreatus* extracts in later experimental assays. The stipe and cap fractions are thus expected to differ in activity according to the concentration and reactivity of the constituent phenolics, as suggested by the electronic structure analysis [23].

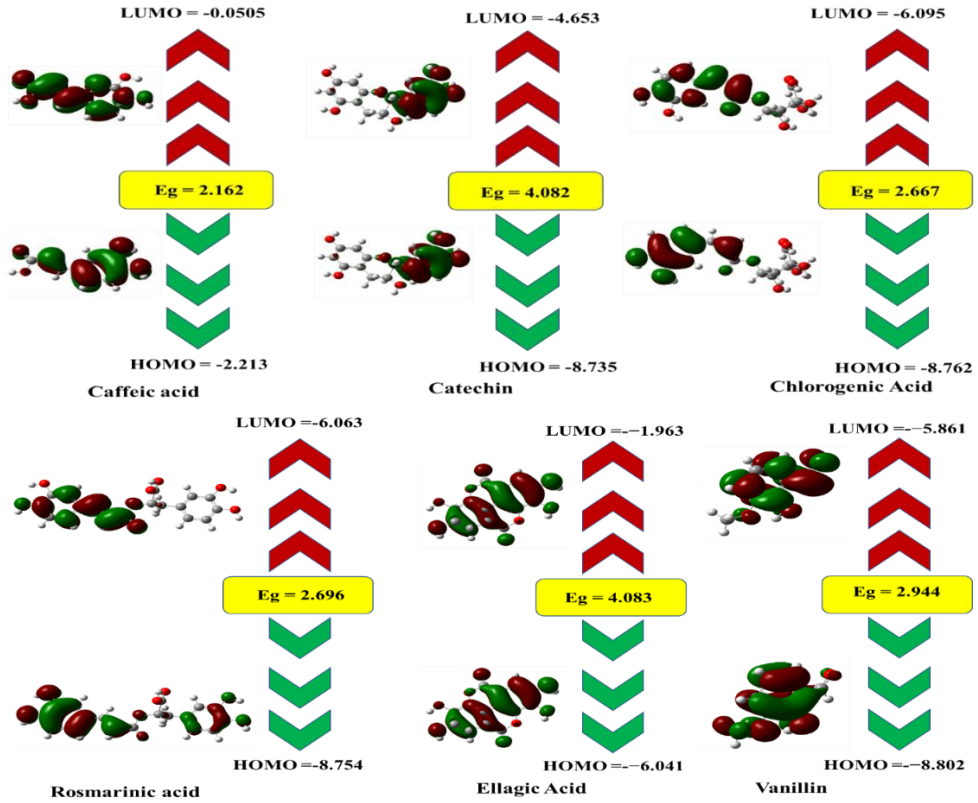

Figure 7. DFT calculations of bioactive compounds.

Molecular docking

Molecular docking analysis of the selected ligands against the Bcl-2 protein (PDB ID: 4IEH) revealed variable binding affinities and interaction patterns within the active site [45]. Bcl-2-IN-13 exhibited the highest binding affinity (−8.0 kcal/mol) and formed five HBs with residue such

as ARG A:66 (2.72 Å), TYR A:67 (2.67 Å), ALA A:59 (3.57 Å), ASP A:70 (3.56 Å), and ASP A:62 (3.42 Å), along with additional interactions involving PHE A:63, ARG A:65, LEU A:96, and ALA A:108. CFA showed a binding affinity of −5.5 kcal/mol and formed one HB with GLY A:104 (3.27 Å), while interacting with ALA A:59, TYR A:161, and VAL A:107. CTC displayed a binding affinity of −6.6 kcal/mol without HB formation, interacting mainly with TYR A:67, PHE A:63, and VAL A:107. CRG demonstrated a binding affinity of −6.8 kcal/mol with one HB involving ARG A:105 (2.12 Å) and additional interactions with PHE A:63 and VAL A:107. ELG showed a binding affinity of −7.4 kcal/mol and formed two HBs with GLY A:104 (2.34 Å) and TYR A:161 (2.90 Å), along with interactions with ASP A:62, ALA A:59, and VAL A:107. GA exhibited a binding affinity of −5.3 kcal/mol and formed one HB with ALA A:59 (2.73 Å), while interacting with PHE A:63, ASP A:62, and VAL A:107. RMC showed a binding affinity of −6.7 kcal/mol and formed three HBs with ASP A:62 (2.84 Å), ALA A:59 (2.51 Å), and GLY A:104 (3.38 Å), along with interactions involving TYR A:161, PHE A:63, and VAL A:107. VNL demonstrated a binding affinity of −5.0 kcal/mol and formed two HBs with ASP A:62 (3.72 Å) and ALA A:59 (2.24 Å), while interacting with TYR A:161 and VAL A:107. However, Table S8 lists the interacting A residues and bond types between the ligand-receptor interactions, and a 3D visualization of the receptor-ligand interaction is depicted in Figure 8.

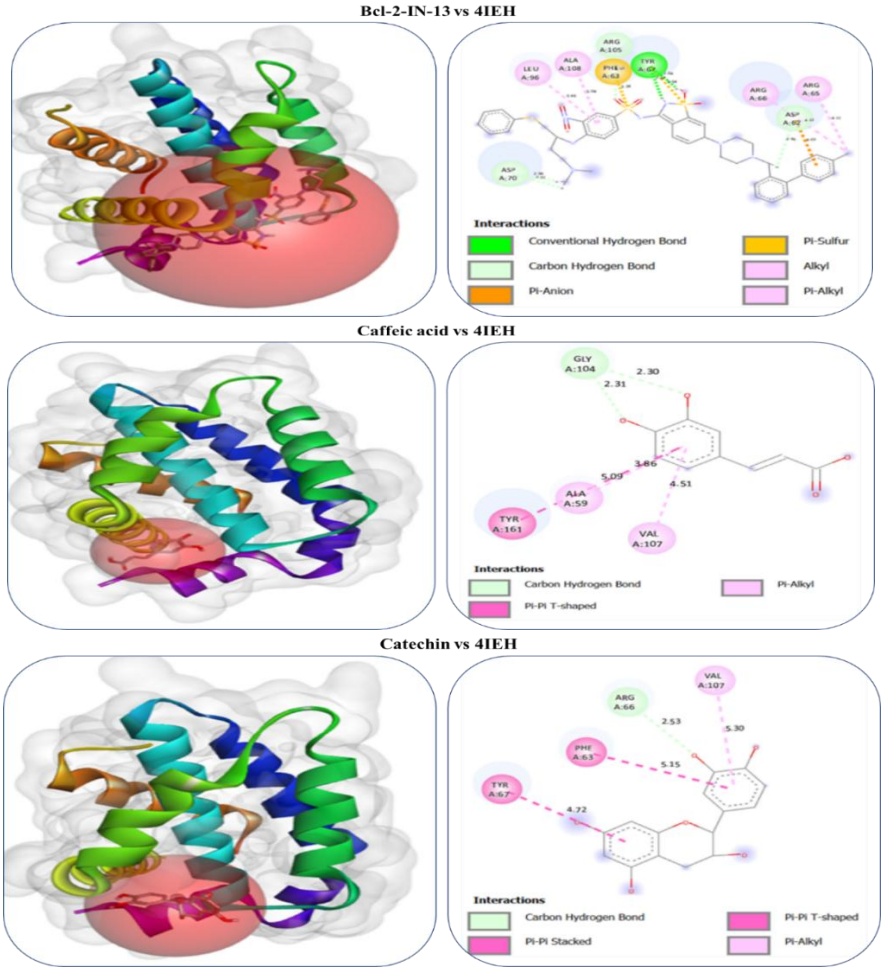

Chlorogenic acid vs 4IEH

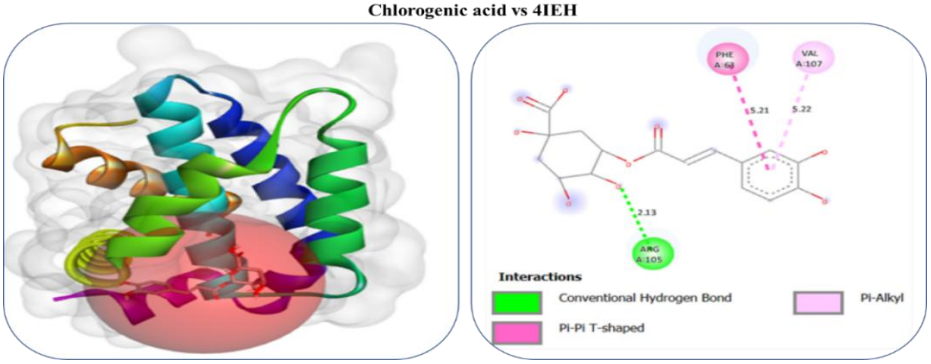

Ellagic acid vs 4IEH

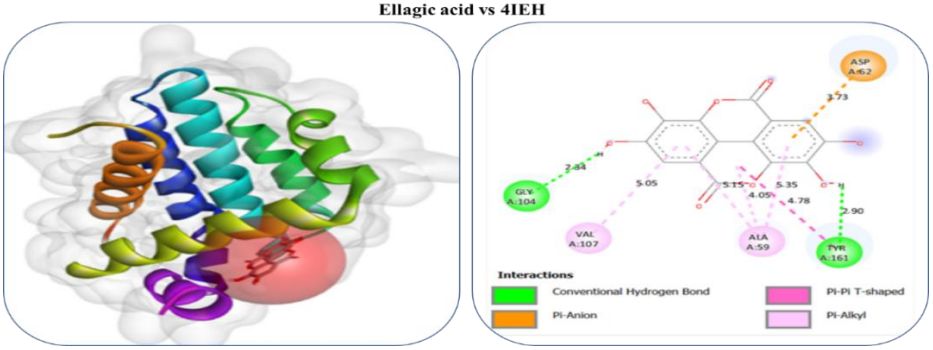

Gallic acid vs 4IEH

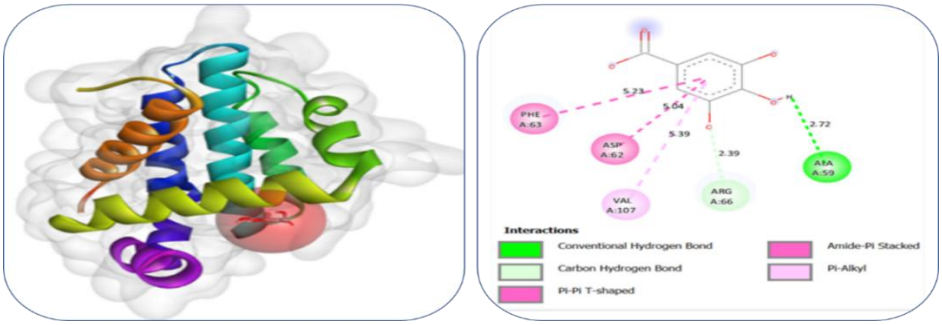

Rosmarinic acid vs 4IEH

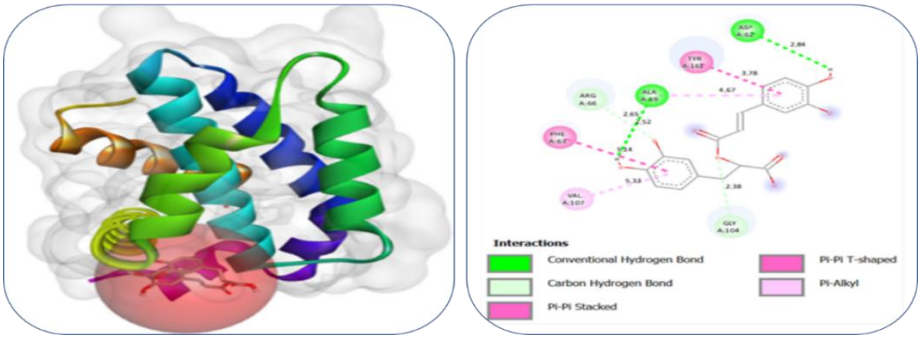

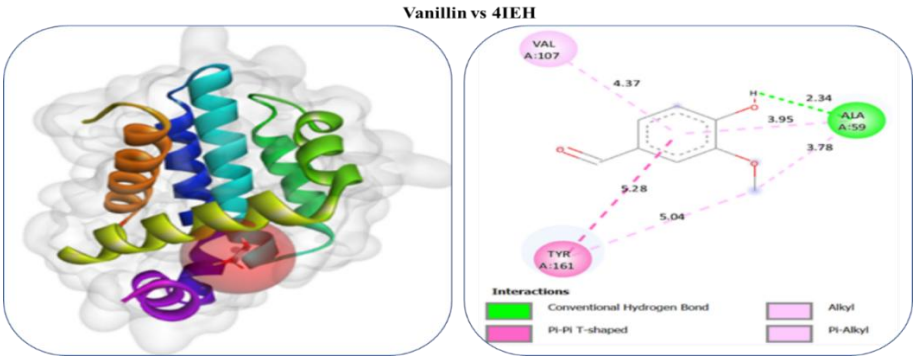

Figure 8. The bond types between the ligand-receptor interactions, and a 3D visualization of the receptor-ligand interaction.

CONCLUSION

This study provides a comprehensive experimental and computational evaluation of the bio functional potential of Libyan wild *P. ostreatus*, with emphasis on tissue-specific differences between the cap and stipe. The main novelty of this work is demonstrating that these two mushroom tissues are not biologically equivalent but instead possess distinct phenolic profiles and functional activities. HPLC-DAD revealed a clear tissue-dependent distribution of phenolic compounds. The cap extract was enriched mainly in chlorogenic and gallic acids, whereas the stipe extract showed a broader phenolic profile dominated by ellagic acid, vanillin, and Rosmarinus acid. These compositional differences were reflected in the biological activities. The cap extract showed stronger antioxidants and cytotoxic effects, which may be related to its higher total phenolic and flavonoid contents. In contrast, the stipe extract showed more pronounced anti-inflammatory activity and measurable antimicrobial effects. However, the antimicrobial findings should be interpreted cautiously because MIC and MBC/MFC values were relatively high compared with standard antimicrobial agents. Both extracts exhibited selective cytotoxicity toward HepG2 hepatocellular carcinoma cells, with lower toxicity toward normal WI-38 fibroblasts. DFT analysis provided insight into the electronic features and reactivity of the major phenolic constituents, while molecular docking suggested favorable interactions with the anti-apoptotic Bcl-2 protein. These computational results support the experimental findings but should be considered predictive and require further biological validation.

ACKNOWLEDGEMENT

The authors gratefully acknowledge their departments for their valuable support and guidance and for providing the facilities and academic environment necessary to carry out this research.

Data availability

All supporting materials are available upon request from the corresponding author.

REFERENCES

1. Sevindik, M.; Karaltı, İ.; Korkmaz, A.F.; Krupodorova, T.; Gürgen, A.; Akata, I. Artificial intelligence-assisted optimization of *Amanita caesarea* extracts for bioactive compounds and functional food applications. *Foods* **2026**, 15, 1896.

2. Raja-Razali, R.B.; Zahia-Azizan, N.A.; Yee, C.S.; Ushidee-Radzi, M.A.; Ilham, Z.; Hamid, N.; Klaus, A.; Wan-Mohtar, W.A.A.Q.I. Lion's mane mushroom: Nutritional profile, bioactive compounds, functional properties, and applications in functional food systems. *J. Food Sci.* **2026**, 91, e71026.
3. Mafe, A.N.; Otieno, C.A.; Edo, G.I.; Akpoghelie, P.O.; Yousif, E.; Isoje, E.F.; Igbuku, U.A.; Ismael, S.A.; Makia, R.S.; Essaghah, A.E.A.; Ahmed, D.S.; Umar, H.; Alamiery, A.A. Domestication and market potential of indigenous mushrooms in Nigeria and Kenya through cultivation techniques, nutritional enhancement, and consumer preference analysis. *Discover Food* **2025**, 5, 248.
4. Haib, S.H.; Kaur, H.; Ben Mohamed, F.E.; Benkhyal, F.A.K.; Bouzid, G.; Belaidi, M.; Ayachi, S.; Ben El Hadj Rhouma, M.; Bogandora, E.S.; Bufarwa, S.M.; Rodriguez-Resendiz, J.; Rojas-Galvan, R.; López-Maldonado, E.A. Evaluation of extraction techniques, chemical composition, antioxidant properties, computational modelling, and biological insights of the novel truffle species (*Tirmania nivea*) for enhanced human health benefits. *Trends Sci.* **2026**, 23, 12762-12762.
5. Ayuso, P.; Quizhpe, J.; Peñalver, R.; García-Pérez, P.; Nieto, G. Green valorization strategies of *Pleurotus ostreatus* and its by-products: A critical review of emerging technologies and sustainable applications. *Molecules* **2025**, 30, 4318.
6. Gómez-Jiménez, M.Á.; Manzano-Gómez, L.A.; Rincón-Molina, C.I.; Gen-Jiménez, A.; Salvador-Morales, P.; Rincón-Molina, F.A.; Acosta-Navarrete, M.S.; Silos-Espino, H.; Maldonado-Gómez, J.C.; Rincón-Rosales, R. Agrobiotechnological potential of *Pleurotus ostreatus* from an ecological–socioeconomic perspective in mexico. *Sustainability* **2025**, 18, 6.
7. Katiyar, D.; Ghosh, D.; Singh, R.; Dixit, S.; Chopra, S.; Tripathi, S.; Saini, T. Medicinal mushrooms: Bioactive components, pharmacological, immunological and toxicological insights. *ChemistrySelect* **2025**, 10, e01956.
8. Warnasooriyaa, W.M.P.B.K.; Chaikaew, A.; Phongthai, S.; Unban, K.; Klangpetch, W.; Khumsap, T.; Rachtanapun, P.; Tangjaidee, P. Bioactive properties of selenium-enriched polysaccharides extracted from *Pleurotus ostreatus* using ultrasonic-assisted extraction. *Curr. Res. Food Sci.* **2025**, 11, 101207.
9. Binsaleh, N.K.; Bazaid, A.S.; Barnawi, H.; Alharbi, B.; Alsolami, A.; Babsail, A.Y.; Selim, S.; Abdelghany, T.M.; Elbaz, R.M.; Qanash, H. Chemical characterization, anticancer, antioxidant and anti-obesity activities with molecular docking studies of *Pleurotus ostreatus* biomass exposed to moist heat. *J. Food Meas. Charact.* **2025**, 19, 1-20.
10. Chaudhary, A.; Maurya, S.; Ehsan, S.; Yadav, P.; Singh, M.P. Pleurotus species: Nutritional powerhouses and biotechnological assets in sustainable fungal research. *World J. Microbiol. Biotechnol.* **2026**, 42, 126.
11. Araújo-Rodrigues, H.; Amorim, M.; de Freitas, V.; Relvas, J.B.; Tavaria, F.K.; Pintado, M. Comparative analysis of polysaccharide and nutritional composition of biological and industrial-scale cultivated *Pleurotus ostreatus* mushrooms for functional food and nutraceutical applications. *Polysaccharides* **2025**, 6, 62.
12. Ferraz, C.G.; Ribeiro, P.R.; Verde, B.V.; Silva, R.S.; Silva, M.C.C.; do Carmo, C.O.; Bazioli, J.M.; dos Santos, I.B.F.; Fill, T.P.; Sforca, M.L.; Silva, F.; Magaton, A.S.; Soares, A.C.F. Metabolite profiling of *Pleurotus ostreatus* grown on sisal agro-industrial waste supplemented with cocoa almond tegument and wheat bran. *Chem. Biodivers.* **2023**, 20, e202300346.
13. Yakobi, S.H.; Nwodo, U.U. Modulation of *Pseudomonas aeruginosa* quorum sensing and biofilm formation by quercetin extracted from *Pleurotus ostreatus*. *Infect. Drug Resist.* **2026**, 19, 568961.
14. Aly, S.H.; Abd El Hafeez, M.S.; Eldahshan, O.A.; Singab, A.N.B. Antioxidant Properties of Phenolic Compounds from Medicinal Plants. In *Phenolic Compounds from Medicinal Plants*, 1st ed., CRC Press: Boca Raton, FL, USA; 2026; pp 60-78.

15. Bolaños-Cardet, J.; Pepió-Tárrega, B.; Saiz-Poseu, J.; López-Moral, A.; Ullah, F.; Yuste, V.J.; Ruiz-Molina, D.; Suárez-García, S. The redox properties of polyphenols and their role in ROS generation for biomedical applications. *Angew. Chem.* **2026**, 138, e13698.
16. Das, A.; Debnath, S.; Pramanik, S.; Monshi, F.I.; Rahimi, M. Bio-digital feedback loop systems: A synergistic integration of predictive genomics, genome editing, and AI-driven phenomic synthesis for next-generation edible and medicinal mushroom breeding. *Antonie van Leeuwenhoek.* **2025**, 118, 168.
17. Baars, J.J.P.; Scholtmeijer, K.; Sonnenberg, A.S.M.; van Peer, A. Critical factors involved in primordia building in Agaricus bisporus: A review. *Molecules* **2020**, 25, 2984.
18. Martinez-Burgos, W.J.; Montes, E.M.; Pozzan, R.; Serra, J.L.; Torres, D.O.; Manzoki, M.C.; Vieira, R.L.; dos Reis, G.A.; Rodrigues, C.; Karp, S.G.; Soccol, C.R. Bioactive compounds produced by macromycetes for application in the pharmaceutical sector: Patents and products. *Fermentation* **2024**, 10, 275.
19. Ali, F.; Bibi, S.; Belaidi, M.; Bufarwa, S.M.; Ashraf, A.; Fatima, H.; Albadrani, G.M.; Al-Ghadi, M.Q.; Altalhi, R.; Abdel-Daim, M.M. Pharmacophore-based discovery of licoisoflavanone as a dual CXCR4/CXCR7 inhibitor for coronary artery disease: Integration of traditional chinese medicine and modern computational approaches. *J. Comput. Biophys. Chem.* **2025**, 25, 1-20.
20. Amin, A.; Fatima, S.; Aslam, M.K.; Belaidi, M.; Bibi, S.; Bufarwa, S.W.; Zahid, S.; Albadrani, G.M.; Altalhi, R.; Sayed, A.A.; Abdel-Daim, M.M. In silico identification of a prognostic gene signature and virtual screening for hepatocellular carcinoma. *Comput. Biol. Chem.* **2025**, 120, 108718.
21. Lozada-Martinez, L.M.; Reyes-Duque, J.D.; Marin-Hamburger, Y.; Lozada-Martinez, I.D. *Pleurotus ostreatus* for environmental remediation and sustainable bioprocesses: An evidence-mapped review of research gaps and opportunities. *J. Fungi*. **2026**, 12, 54.
22. Bufarwa, S.M.; Belaidi, M.; Abbass, L.M.; Thbayh, D.K. Anticancer activity, DFT, molecular docking, ADMET, and molecular dynamics simulations investigations of Schiff base derived from 2, 3-diaminophenazine and its metal complexes. *Appl. Organomet. Chem.* **2025**, 39, e7953.
23. Hasan, H.; Almabruk, A.M.A.; Belaidi, M.; Bufarwa, S. Dieckol from brown algae targeting the hepatocellular carcinoma pathway: A computational pharmacology study. *Pharmacological Res. Rep.* **2025**, 4, 100064.
24. Hussein, M.A.; Munirathinam, G. Artificial intelligence-driven natural product discovery for cancer metastasis and chemoresistance: From computational prediction to preclinical validation. *Cancers* **2026**, 18, 719.
25. Mustapha, B.; Saleh, A.A.; El-Seifat, R.; Bufarwa, S.; Hasan, H.; Moustafa, D. Exploring the antituberculosis, anti-inflammatory, and antimicrobial activities and computational potential of quinoline-8-ol azo dye complexes. *Appl. Organomet. Chem.* **2025**, 39, e70310.
26. Alsaeedi, M.S. Design of deep-blue emitting iridium complexes with diamine ancillary ligands: hydrophobic and π-stacking effects from experimental and DFT studies. *Bull. Chem. Soc. Ethiop.* **2026**, 40, 1679-1690.
27. Aldujaili, R.A.B.; Ghafil, R.A.; Mohsein, H.F.; Abd Wannas, F.; Azooz, E.A. Effective design, spectroscopic characterization, antifungal activity, and computational analysis of new pyrazole and tetrazole derivative compounds. *Bull. Chem. Soc. Ethiop.* **2026**, 40, 271-281.
28. Azooz, E.A.; Abduladheem, N.A.; El Abbadi, N.K. An overview of the green synthesis of coinage metallic nanoparticles: protocols, challenges, and cancer treatments. *Nano Life* **2025**, 15, 2430011.
29. Venkatesh, G.; Mammadova, K.; Aslanova, A.; Ayyar, M.; Balasubramaniyan, S.; Vennila, P. Synthesis and biological evaluation of novel thiazolidine-2,4 dione derivatives: Computational and experimental studies. *Bull. Chem. Soc. Ethiop.* **2026**, 40, 1557-1568.

30. Zhu, W.; Hu, J.; Li, Y.; Yang, B.; Guan, Y.; Xu, C.; Chen, F.; Chi, J.; Bao, Y. Comparative proteomic analysis of *Pleurotus ostreatus* reveals great metabolic differences in the cap and stipe development and the potential role of Ca^{2+} in the primordium differentiation. *Int. J. Mol. Sci*. **2019**, 20, 6317.
31. Dhanesh, P.; Ajithkumar, T. In vitro anti-inflammatory and antitubercular studies of various extracts of *Abutilon indicum* (L.) sweet leaves. *J. Pharm. Sci*. **2025**, 7, 256-260.
32. Abbass, L.M.; Yousif, N.M.; Sadeek, S.A.; Zordok, W.A.; El-Attar, M.S.; El-Farargy, A.F.; Mouneir, S.M. Structural characterization, XRD, DFT calculations, docking, antimicrobial, anticancer applications, and electrochemical performance studies of some new Schiff base transition metal complexes. *Appl. Organomet. Chem.* **2025**, 39, e70099.
33. Oluoch, M.A.; Onyango, B.O.; Bulli, P. Interactive effects of environment on antimicrobial activity of extracts of the termite *Macrotermes subhyalinus* (Blattodea: Termitidae). *J. Insect Sci.* **2025**, 25, ieaf075.
34. Farouk, H.M.; Attia, E.Z.; Shaban, G.M.; Abdelmohsen, U.R.; El-Katatny, M.M.H. Antimicrobial secondary metabolites and antioxidant activities of fungal endophytes associated with *Ziziphus spina-christi* (L.) Desf. (Nabq) leaves. *Nat. Prod. Res.* **2025**, 39, 4788-4792.
35. Duangsombat, P.; Waranuch, N.; Pitaksuteepong, T. Chemical characterization and antimicrobial activities of *Citrus aurantifolia* peel oils and *Ocimum sanctum* ethanolic extract. *PLoS One*. **2025**, 20, e0331710.
36. Diment, D.; Musl, O.; Balakshin, M.; Rigo, D. Guidelines for evaluating the antioxidant activity of lignin via the 2,2-diphenyl-1-picrylhydrazyl (DPPH) assay. *ChemSusChem.* **2025**, 18, e202402383.
37. Laria, F.Y.; Belaidi, M.; Mohammed, H.S.; Bufarwa, S.M.; El-Ajaily, M.M.; Abbass, L.M. Preparation, identification, and antimicrobial analysis, molecular docking, molecular dynamics simulation, ADMET, DFT, of dual-ligand complexes of Schiff bases with M(III) ions (M= Fe, La, and Cr). *J. Comput. Biophys. Chem.* **2025**, 25, 2673-2694.
38. Nath, A.R.; Kumar, M.; Ali, M.E. Intramolecular magnetic exchange interaction in dichalcogenide substituted organic diradical dications. *J. Chem. Theory Comput.* **2025**, 21, 168-1694.
39. Bakheit, A.H.; Abuelizz, H.A.; Al-Salahi, R. Crystallographic analysis, Hirshfeld surface investigation, and DFT calculations of 2-phenoxy-triazoloquinazoline molecule: Implications for drug design. *J. Mol. Struct.* **2025**, 1319, 139436.
40. Kaifi, I.; Muhammad, S.; Bibi, S.; urRehman, S.; Kalam, A.; Chaudhry, A.R.; Alarfaji, S.S.; Al-Sehemi, A.G. Optimizing core modifications for high-performance D-A-D molecular systems: A multi-faceted study on NLO properties, solvent effects, charge transfer, and photovoltaic efficiency. *Adv. Theory Simul.* **2025**, 8, 2500169.
41. Venkatesh, R.; Murugan, T.; Kubaib, A.; Umamaheswari, L.; Imran, P.M.; AbdelGawwad, M.R.; Alayadi, H.; Alfrisany, N.M. Exploring the chemical and biological landscape of a nickel(II) Schiff base complex via azomethine linkage. *Sci. Rep.* **2026**, 16, 2256.
42. Ekeocha, C.I.; Uzochukwu, I.N.; Onyeachu, I.B.; Etim, I.I.N.; Oguzie, E.E. Theoretical study of novel antipyrine derivatives as promising corrosion inhibitors for mild steel in an acidic environment. *Struct. Chem.* **2025**, 36, 363-379.
43. Islam, M.T.; Hasan, M.S.A.; Ferdous, J.; Alshahrani, M.Y.; Mia, E.; Jony, M.A.; Shipon, M.N.H.; Hasan, A.M.W.; Saifuzzaman, M. Anxiolytic-like effects of citronellal and phytol, possibly through the GABAergic interaction pathway: in vivo with molecular docking studies. *Mol. Neurobiol.* **2026**, 63, 104.
44. Gunasekaran, V.; Dhakshinamurthy, S.S. Computational insights into the interaction of pinostrobin with Bcl-2 family proteins: A molecular docking analysis. *Asian Pac. J. Cancer Prev.* **2024**, 25, 507.

45. Rakib, I.H.; Khan, M.S.; Ayub, A.; Al Hasan, M.S.; Alfaifi, M.; Bhuia, M.S.; Mia, E.; Yana, N.T.; Shipon, M.N.H.; Islam, M.T. Salvianolic acid A enhances sedative effect of diazepam through the GABAergic pathway: In vivo, molecular docking, and pharmacokinetics approaches. *Neurotoxicol. Teratol.* **2025**, 110, 107517.
46. Jahan, N.; Mandal, M.; Rakib, I.H.; Al Hasan, M.S.; Mia, E.; Yana, N.T.; Alfaifi, M.; Altemani, F.H.; Hossan, R.; Sumaya, U.H.; Hasan, A.M.W.; Sayeed, M.A.; Mou, M.A.; Islam, M.T.; Bhuia, M.S. Oleuropein modulates anti-inflammatory activity of celecoxib and ketoprofen through cyclooxygenase pathway: *In vivo*, in silico and pharmacokinetics approaches. *Naunyn-Schmiedeberg's Arch. Pharmacol.* **2025**, 398, 16195-16208.
47. Fahmi, A.A.; Akter, K.; Rakib, I.H., Hossain, S.; Alkhathami, A.G.; Al Hasan, M.S.; Hossan, R.; Ara, I.; Rahaman, M.M.; Islam, T.M. Linalool exerts antiemetic effects via dopaminergic and serotonergic pathways: Evidence from chick model and molecular docking. *Naunyn-Schmiedeberg's Arch. Pharmacol.* **2025**, 399, 4401-4411.
48. Ahmmed, M.S.; Munshi, M.H.; Yana, N.T.; Rakib, I.H.; Mia, E.; Tohfa, N.J.; Al Hasan, M.S.; Sayeed, M.A.; Akter, M.S.; Hossain, M.A.; Islam, M.T.; Bhuia, M.S.; Ansari, M.A. Assessment of antiemetic potential of schaftoside through modulation of dopaminergic, serotonergic and muscarinic signaling pathways: *In vivo* and in silico investigations. *Naunyn-Schmiedeberg's Arch. Pharmacol.* **2025**, 399, 4267-4283.
49. Xu, W.; Lucke, A.J.; Fairlie, D.P. Comparing sixteen scoring functions for predicting biological activities of ligands for protein targets. *J. Mol. Graph. Model.* **2015**, 57, 76-88.